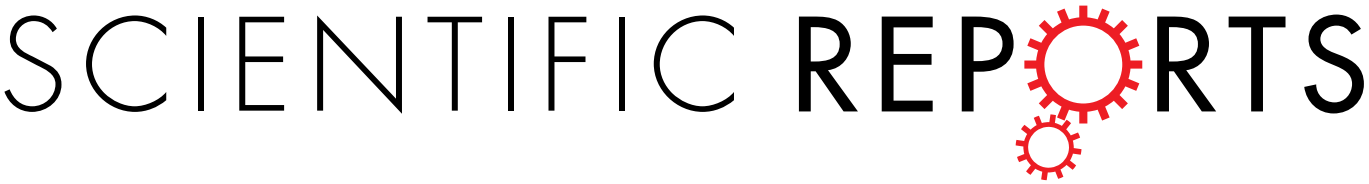

OPEN

Received: 30 November 2016
Accepted: 30 January 2017
Published: 26 April 2017

Ordered micro/macro porous K-OMS-2/SiO_2 nanocatalysts: Facile synthesis, low cost and high catalytic activity for diesel soot combustion

Xuehua Yu[1], Zhen Zhao[1,2], Yuechang Wei[2] & Jian Liu[2]

A series of novel oxide catalysts, which contain three-dimensionally ordered macroporous (3DOM) and microporous structure, were firstly designed and successfully synthesized by simple method. In the as-prepared catalysts, 3DOM SiO_2 is used as support and microporous K-OMS-2 oxide nanoparticles are supported on the wall of SiO_2. 3DOM K-OMS-2/SiO_2 oxide catalysts were firstly used in soot particle oxidation reaction and they show very high catalytic activities. The high activities of K-OMS-2/SiO_2 oxide catalysts can be assigned to three possible reasons: macroporous effect of 3DOM structure for improving contact between soot and catalyst, microporous effect of K-OMS-2 for adsorption of small gas molecules and interaction of K and Mn for activation of gas molecules. The catalytic activities of catalysts are comparable to or even higher than noble metal catalyst in the medium and high temperature range. For example, the T_{50} of K-OMS-2/SiO_2-50, 328 °C, is much lower than those of Pt/Al_2O_3 and 3DOM Au/$LaFeO_3$, 464 and 356 °C,respectively. Moreover, catalysts exhibited high catalytic stability. It is attributed to that the K^+ ions are introduced into the microporous structure of OMS-2 and stabilized in the catalytic reaction. Meanwhile, the K^+ ions play an important role in templating and stabilizing the tunneled framework of OMS-2.

Soot particles derived from the exhaust of diesel engine are a kind of main source of urban atmospheric particulate matters, which is directly threatening environment and people's health[1,2]. Therefore, elimination of soot particles is urgent for the protection of environment. In previous studies, many techniques have been developed for solving pollution of diesel engine exhaust, and the after-treatment of diesel exhaust is one of the most perspective techniques[3,4]. The process of soot combustion is a catalytic reaction involving three phases of gas(O_2)-solid(soot)-solid(catalyst)[5]. It is affected by two factors: the contact condition between soot and catalyst, and the intrinsic activity of catalyst. Therefore, design and preparation of catalysts, which can effectively enhance contact area and intrinsic activity of catalysts, is significant for soot combustion.

Due to smaller pore sizes (<10 nm) of traditional catalysts than soot particles (>20 nm), it is difficult for soot particles to enter inner pores of these catalysts so that their catalytic activities are limited[6]. Thus, finding novel catalysts, which can effectively make use of inner surface for increasing the contact area between catalysts and soot particles, is a key factor affecting the catalytic activity for soot combustion. Recently, three-dimensionally ordered macroporous (3DOM) oxides have been considered as potential catalysts owing to uniform pore size (>50 nm) and well-defined structure[7–9]. The soot particles not only could enter their inner pores more easily, but also could access the active sites more flexibly than nanoparticle samples when 3DOM materials are taken as catalysts for soot combustion. In our previous studies, a series of 3DOM metal mixed oxides, including $La_{1-x}K_xCoO_3$[10] and $Ce_{1-x}Zr_xO_2$[11] and so on, have been prepared and they all show better catalytic performances than the corresponding nanoparticle catalysts for soot oxidation. However, because of limitation of intrinsic activity, 3DOM

[1]Institute of Catalysis for Energy and Environment, College of Chemistry and Chemical Engineering, Shenyang Normal University, Shenyang, Liaoning, 110034, China. [2]State Key Laboratory of Heavy Oil Processing, China University of Petroleum, 18# Fuxue Road, Chang Ping, Beijing 102249, China. Correspondence and requests for materials should be addressed to Z.Z. (email: zhaozhen@synu.edu.cn or zhenzhao@cup.edu.cn)

oxide-based catalysts do not show high enough activity for soot oxidation at low temperature. In order to further improve the intrinsic activity of catalysts for soot combustion, the advantages of supported noble metal (Au, Pt, Pd, Ag, etc) nanoparticles (NPs) catalysts have been recognized[12,13]. We have synthesized several kinds of 3DOM oxides-supported Au and Pt catalysts[14]. Those 3DOM oxides-supported noble metal catalysts exhibit high catalytic activities for soot combustion. However, noble metal catalysts are very expensive than metal oxide catalysts, which restricts the extensive employment of noble metal catalysts.

Novel catalysts with low cost and fine intrinsic activity are significant for practical application[15,16]. Due to three phases of gas (O_2)-solid (soot)-solid (catalyst) for catalytic soot combustion, adsorption and activation of small gas molecules is also important to enhance the catalytic activity[17,18]. 3DOM wall structure is in favor of soot transmission while it has disadvantage for adsorption of small gas molecules. Herein supporting microporous structure materials on the 3DOM wall structure could enhance the catalytic activity by macroporous effect for soot transmission and microporous effect for adsorption and activation of small gas molecules. Recently, researchers demonstrated that cryptomelane-type manganese oxide (e.g., manganese oxide octahedral molecular sieve (OMS-2)) has a microporous structure (0.46 nm) arising from edge sharing of 2×2 [MnO_6] octahedral chains to form one-dimensional tunnel structures[19]. More importantly, OMS-2 have mixed valence states of Mn^{4+}, Mn^{3+} and/or a small amount of Mn^{2+} sites. The manganese oxides with multiple Mn oxidation states have been reported as promising catalysts for oxidation reactions[20]. In addition, potassium (K)-containing materials, which can increase chemisorbed oxygen, form eutectic compounds and carbonate intermediates, show better catalytic performance for soot combustion than other alkali elements[21,22]. However, the catalytic activities of K-based catalysts usually tend to degrade after repeated thermal cycles owing to the loss of potassium. Incorporation of K into a more stable structure is one of effective approaches[23,24]. Many K-doped catalysts, including K-doped perovskite catalysts[25], and K-doped single metal oxides[26,27], have been studied for soot combustion. Because the tunnel cavity of OMS-2 is as large as 0.46 nm, some large cations, such as K^+, Na^+, Ba^{2+} and others, are inevitably introduced into the tunnel and stabilized in the catalytic reaction[28]. More interestingly, the K^+ ion plays an important role in templating and stabilizing the tunneled framework of OMS-2[29]. Due to changing valence states of Mn species in the OMS-2 and high catalytic activity of K for soot combustion, microporous K-OMS-2, which are formed nanoparticles and supported on 3DOM SiO_2, are expected to enhance catalytic performance for soot combustion by macroporous effect, microporous effect, nano-effect and synergistic effect between K and Mn.

In this paper, a series of novel oxide catalysts, which contain 3DOM structure in the SiO_2 support and microporous structure in the nano-K-OMS-2, were firstly designed and prepared by a very simple method. The as-prepared catalysts exhibit super high catalytic activities for soot combustions owing to macroporous structure for soot transmission and micropore structure for the activation of small molecules (NO, O_2). More interestingly, the as-prepared catalysts adopt cheap KNO_3 and $Mn(NO_3)_2$ materials as active components, thus they cost much lower than noble metal catalysts. They show similar or even higher catalytic activities in medium temperature rage. In addition, the influence of NO and stability of as-prepared catalysts were also studied. The possible mechanisms of catalysts for soot combustion are discussed based on the results of characterization.

Results

Structural Features of As-prepared Catalysts. The XRD patterns results of as-prepared catalysts are shown in the Fig. 1. The Fig. 1a shows the diffraction peaks of pure SiO_2, which the 23.5° is corresponding to the amorphous SiO_2. As shown in Fig. 1b–h, the feature peaks, which 2θ degree are located at 12.6°, 28.6°, 37.4°, 41.6°, are corresponding to cryptomelane-M (OMS-2) with a space group of I2/m(12) (JCPDS Card No. 44-1386) and they increased with increasing of K-OMS-2 loading amounts (as "▲" marked in the Fig. 1b–h). Figure 1i suggests that the cryptomelane-M is also synthesized on the surface of silica gel support. Different active components supported on 3DOM SiO_2 show various feature peaks. The feature peaks (as "■" marked in the Fig. 1j) could be readily indexed to manganese oxides[13]. Those feature peaks, which marked by the "★" in the Fig. 1k, are corresponding to the diffraction peaks of KNO_3. Different XRD patterns of as-prepared catalysts indicate that the potassium has been doped into the tunnel structure of OMS-2. The above results illustrate that we have successfully prepared a novel ordered micro/macro catalyst, which contains 3DOM SiO_2 and microporous structure in K-OMS-2 NPs.

The SEM images (Fig. 2) clearly demonstrate that all 3DOM K-OMS-2/SiO_2 catalysts have long range ordered macroporous with average diameter of ca. 310 ± 20 nm. As shown in the Fig. 2b–h, more and more visible nanoparticles can be obtained on the skeleton of 3DOM SiO_2 when the loadings of K-OMS-2 NPs are increased. Especially, when the loading of K-OMS-2 is higher than a certain value (K-OMS-2/SiO2–60), the surface of 3DOM SiO_2 is completely covered by K-OMS-2 NPs and the pores of 3DOM SiO_2 were also filled (Fig. 2h). Combined with the XRD results (Fig. 1a–h), the K-OMS-2 NPs, which supported on the surface of 3DOM SiO_2, would be contributed to enhancing the intensity of diffraction peaks for cryptomelane-M. In order to compare the influence of different active components and supports, the SEM images of K-OMS-2/silica gel, MnO_x/SiO_2-50 and KNO_3/SiO_2-50 are also exhibited in the Supporting information. As shown in the Fig. S2, K-OMS-2/silica gel is constituted by nanoparticles (Fig. S2a). SEM images of MnO_x/SiO_2-50 and KNO_3/SiO_2-50 (Fig. S2b and c) indicate that 3DOM SiO_2 is stable when different active components supported on the surface of 3DOM structure.

TEM images of 3DOM K-OMS-2/SiO_2 catalysts are shown in the Fig. 3. From the Fig. 3a, no any K-OMS-2 NPs are covered on the skeleton of 3DOM SiO_2. However, as shown in Fig. 3b–h, the surface of 3DOM SiO_2 is successfully decorated with well-dispersed K-OMS-2 NPs and no larger agglomerated particles is observed. The average K-OMS-2 NPs sizes are estimated to be 20–25 nm for 3DOM K-OMS-2/SiO_2 catalysts with different K-OMS-2 loadings (see in the Fig. S5). The densities of K-OMS-2 NPs on the skeleton of 3DOM SiO_2 are increased with the enhancement of loading dosages of active components. TEM images of Fig. 3g and h exhibit that the surface of 3DOM SiO_2 is completely covered by K-OMS-2 NPs, which is agreed with the SEM results (Fig. 2). Figure S3 shows TEM images of catalysts with different supports and active components. It indicates that

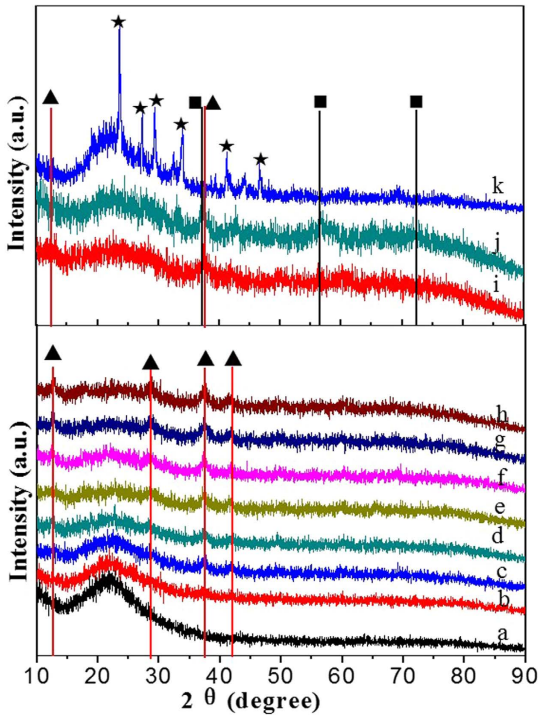

Figure 1. XRD patterns of as-prepared catalysts. SiO_2 (**a**); K-OMS-2/SiO_2-10 (**b**); K-OMS-2/SiO_2-20 (**c**); K-OMS-2/SiO_2-30 (**d**); K-OMS-2/SiO_2-40 (**e**); K-OMS-2/SiO_2-50 (**f**); K-OMS-2/SiO_2-60 (**g**); K-OMS-2/SiO_2-70 (**h**); K-OMS-2/Silica gel-50 (**i**); MnO_x/SiO_2-50 (**j**); KNO_3/SiO_2-50 (**k**).

the silica gel is composed of SiO_2 particles, and no obvious particles of K-OMS-2 are observed on the silica gel (Fig. S3a). The reason for this phenomenon is that the precursor solution of KNO_3 and $Mn(NO_3)_2$ is infiltrated into the inner of silica gel through accumulation pores. Figure S3b shows the TEM image of MnOx/SiO_2-50. The surface of 3DOM SiO_2 is covered by nanoparticles of MnO_x, which the particle size is about 22 nm (Fig. S5h). As shown in the Fig. S3c, no particles of KNO_3 appeared on the surface of 3DOM SiO_2.

The HRTEM images of as-prepared catalysts with different supports and active components are shown in Fig. 4. HRTEM image of K-OMS-2/SiO_2-50 shows that the lattice fringes of K-OMS-2 NPs are clearly observed (Fig. 4a), e.g. the interplanar spacing is measured to be 0.463 nm indexed as (002) planes of K-OMS-2. As shown in the Fig. S4a–g, clear lattice fringes can be observed on the K-OMS-2/SiO_2 with various K-OMS-2 loadings. The lattice fringes are corresponding to the crystal of K-OMS-2. Those results indicate that K-OMS-2 nanoparticles contain a microporous structure (0.46 nm) arising from edge sharing of 2×2 [MnO_6] octahedral chains to form one-dimensional tunnel structures (as shown insert of Fig. 4a)[20]. Because the tunnel cavity of OMS-2 is as large as 0.46 nm, the K^+ cations are inevitably introduced into the tunnel and stabilized in the catalytic reaction. From the Fig. 4b, the irregular K-OMS-2 particles are appeared on the surface and inner of silica gel. And the lattice fringes was measured to be 0.465 nm indexed as (002) planes of K-OMS-2. As shown in the Fig. 4c, the distinct lattice fringes (0.489 nm) are assigned to the (200) planes of manganese oxides. Figure 4d shows an interesting result of KNO_3/SiO_2-50, no particles or sheets of KNO_3 can be observed on the surface of SiO_2, indicating that the KNO_3 may be adhered on the surface of SiO_2 with molten state during the calcined process. After finishing of calcined process, the KNO_3 are uniform distributed on the skeleton of SiO_2.

In order to get the distributed information of K, Mn, O and Si elements in the as-prepared catalysts, the HAADF-STEM image and EDS elemental mapping of K-OMS-2/SiO_2-50 are shown in the Fig. 5. The EDX elemental mappings suggest that the O and Si are uniformly distributed in the in the αorts of 3DOM SiO_2. Due to O element in the K-OMS-2 NPs, the O element can be found more riches in the K-OMS-2 NPs while the Si element cannot be obviously observed in the K-OMS-2 NPs. As shown in the Fig. 5, the Mn element is aggregated in the K-OMS-2 NPs owing to Mn is the main components for K-OMS-2 NPs. In addition, the K element is also focused on the K-OMS-2 NPs. However, the intensity of K element is seemed weaker than corresponding that of Mn element. The possible reason for this phenomenon is that the K elements are doped into the one-dimensional tunnel structures of 2×2 [MnO_6] octahedral chains.

TGA-DSC Analyses of As-prepared Catalysts. The weight loss and heat flow of K-OMS-2/SiO_2-50 samples (none calcined and calcined) observed during thermogravimetry-differential thermal analyses (TGA-DSC) in an oxygen atmosphere are displayed in Fig. 6. As shown by the TGA curve of none calcined K-OMS-2/SiO_2-50 (Fig. 6A), weight losses occurred in three temperature ranges of 50–250, 250–600 and 600–1000 °C. The first significant weight loss of 31.3% is mainly attributed to the decomposition of KNO_3 and $Mn(NO_3)_2$. In this process, the K and Mn ions are formed impermanent species of K-OMS-2, so that the NO_3^- in the KNO_3 is separated and

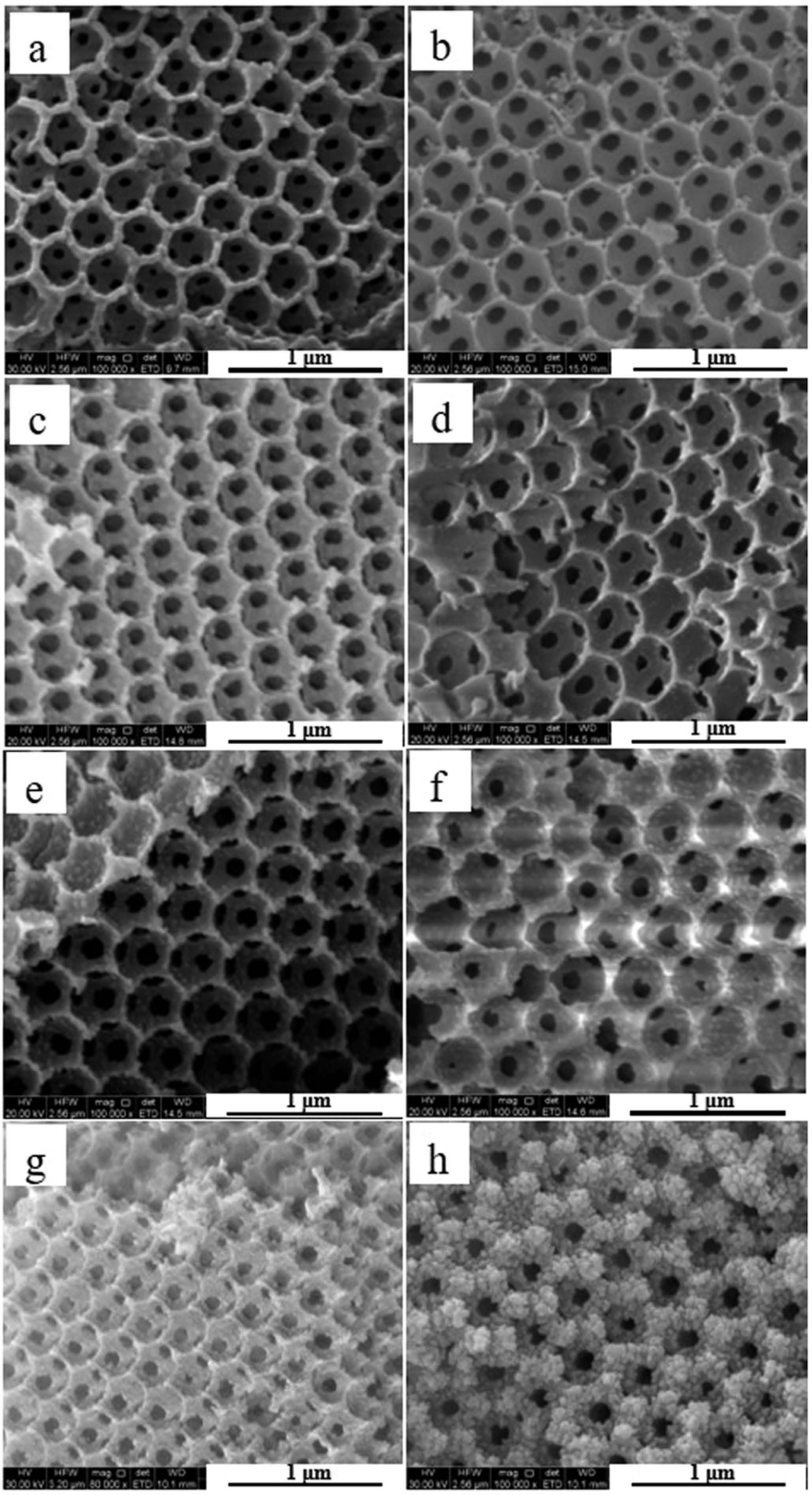

Figure 2. SEM images of 3DOM K-OMS-2/SiO_2. SiO_2 (**a**); K-OMS-2/SiO_2-10 (**b**); K-OMS-2/SiO_2-20 (**c**); K-OMS-2/SiO_2-30 (**d**); K-OMS-2/SiO_2-40 (**e**); K-OMS-2/SiO_2-50 (**f**); K-OMS-2/SiO_2-60 (**g**); K-OMS-2/SiO_2-70 (**h**).

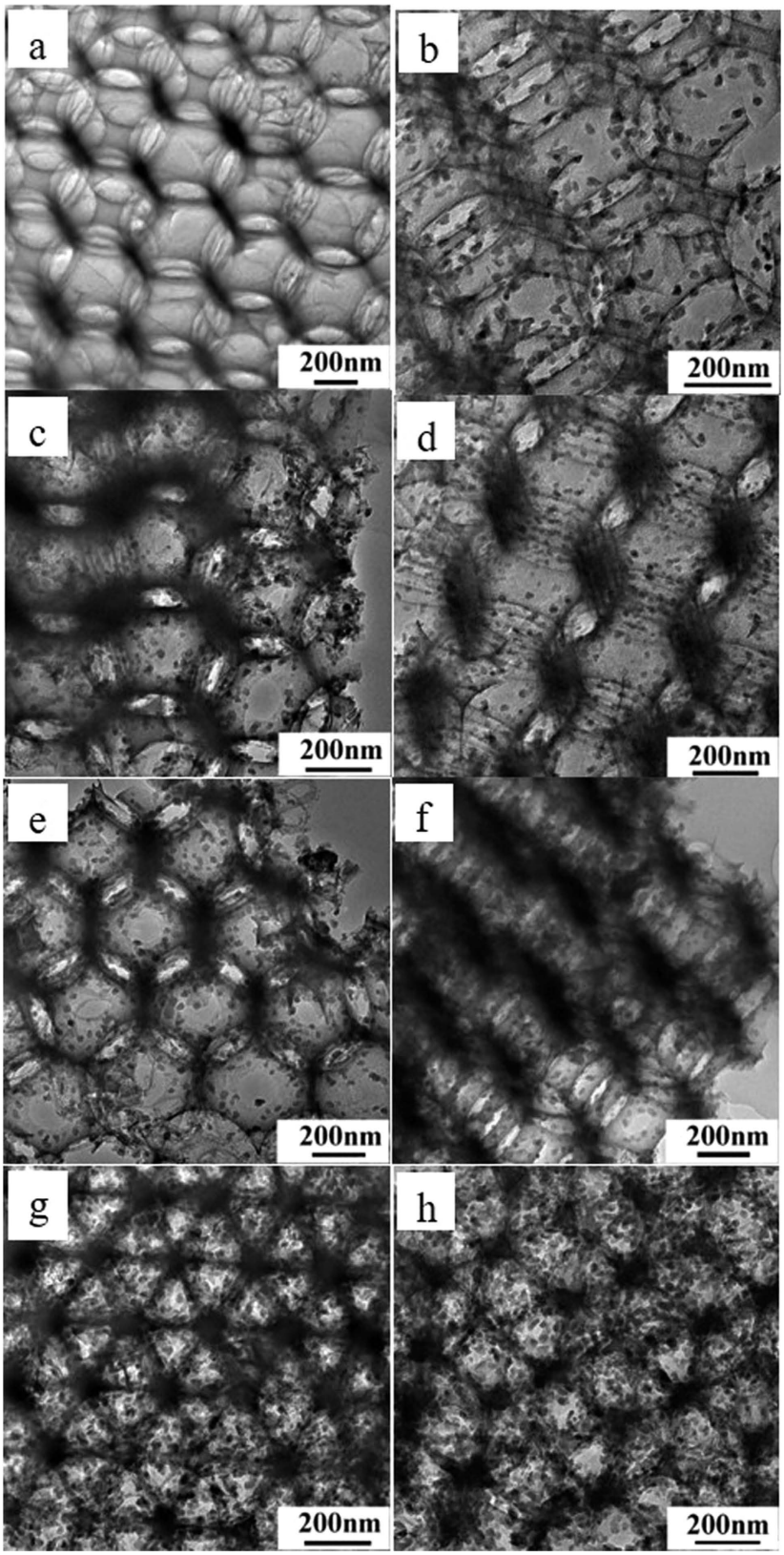

Figure 3. TEM images of 3DOM K-OMS-2/SiO_2 catalysts. SiO_2 (**a**); K-OMS-2/SiO_2-10 (**b**); K-OMS-2/SiO_2-20 (**c**); K-OMS-2/SiO_2-30 (**d**); K-OMS-2/SiO_2-40 (**e**); K-OMS-2/SiO_2-50 (**f**); K-OMS-2/SiO_2-60 (**g**); K-OMS-2/SiO_2-70 (**h**).

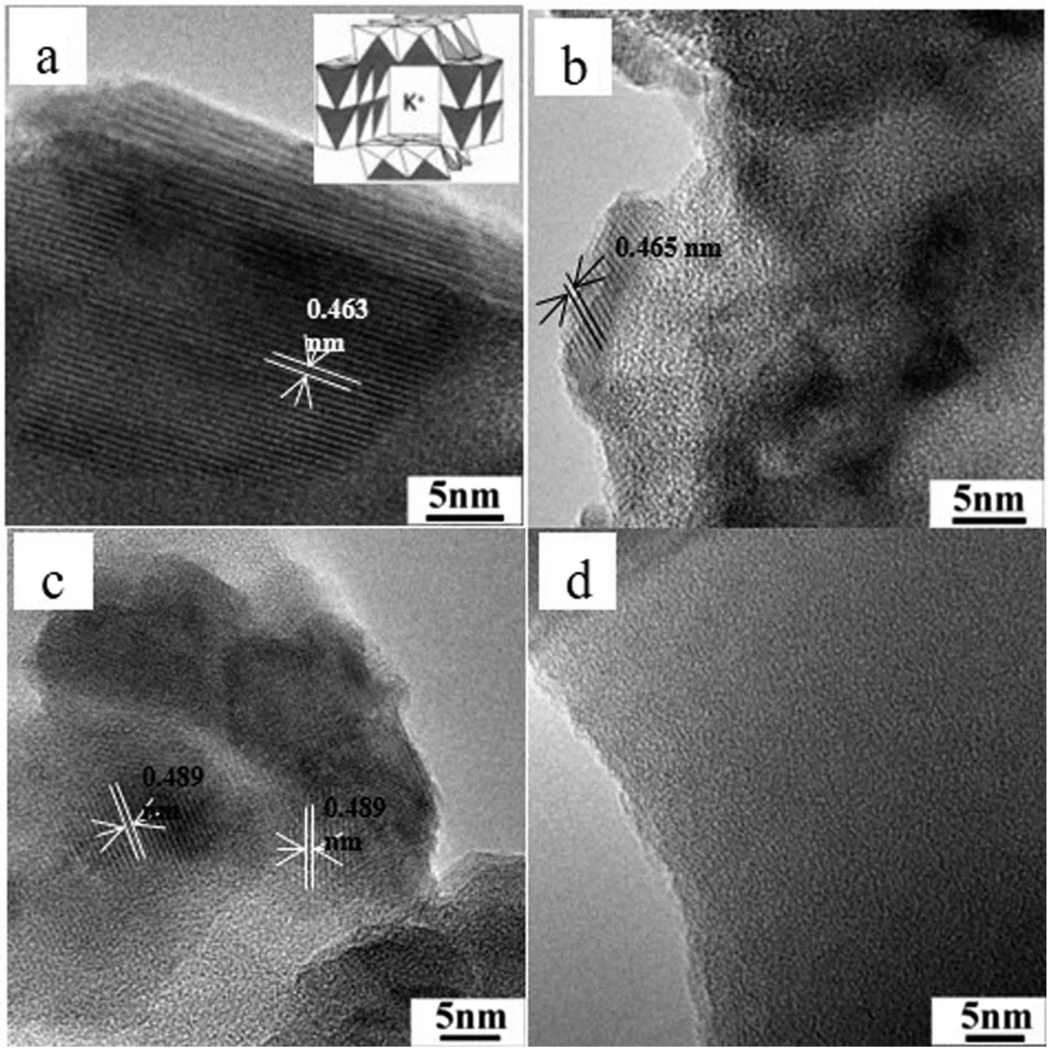

Figure 4. HRTEM images of K-OMS-2/SiO_2-50 (**a**), K-OMS-2/Silica gel-50 (**b**), MnO_x/SiO_2-50 (**c**) and KNO_3/SiO_2-50 (**d**).

decomposed. Certainly, desorption of physisorbed and chemisorbed water is also contributed to the first significant weight loss. The second significant weight loss of 4.2% in the temperature range of 250–600 °C is generally due to further dehydration, lattice oxygen loss or part nitrate decomposition of K-OMS-2. The third slight weight loss of 2.1% is started at 600 °C and ended at 1000 °C. In this temperature range, the collapse and the change of K-OMS-2 to hausmannite by the transformation of Mn^{4+} to Mn^{3+} are the possible reasons for lattice oxygen release[30]. As you can see from the DSC curve of none calcined K-OMS-2/SiO_2-50, a small exothermic peak appeared in the range of 120–180 °C with the highest exothermic value at ca. 160 °C. This exothermic peak reveals the thermal decomposition of nitrate, which came from the preparation process. With increasing of temperature, as a result of dehydration and crystal phase transformation, an endothermic process appears in the DSC curve when the temperature is over 250 °C. Another small exothermic peak at 830 °C is corresponding to crystal change of K-OMS-2[31]. Figure 6B shows the TGA-DSC curves of calcined K-OMS-2/SiO_2-50. Compared with TG curve of none calcined K-OMS-2/SiO_2-50, the calcined K-OMS-2/SiO_2-50 has less weight loss owing to decomposition of nitrate in the calcination process. The weight loss also could be divided into three parts in the range of 50-1000 °C. The temperatures of the first weight loss are in the range of 50–250 °C. Because the nitrate has been decomposed in the calcination process, the first weight loss about 2.4% can be attributed to desorption of physisorbed and chemisorbed water. The second weight loss is occurred in the temperature range of 250–600 °C and the ratio of weight loss is 0.5%. Similarly, further dehydration and lattice oxygen loss of K-OMS-2 may be contributed to this weight loss. The third weight loss is 2.9% and temperature range is 600–1000 °C[32]. The reasons for this weight loss are similar to that of none calcined K-OMS-2/SiO_2-50. As shown in Fig. 6B, compared with DSC curve in the Fig. 6A, the DSC curve of calcined K-OMS-2/SiO_2-50 indicates that no exothermic peak appears in the range of 120–180 °C due to no nitrates in the calcined sample. However, the curve of calcined K-OMS-2/SiO_2-50 is the same as that of none calcined K-OMS-2/SiO_2-50 when the temperature is over 250 °C. An overview of TG-DSC characterizations indicates that the as-prepared catalysts are stable under the calcination temperature

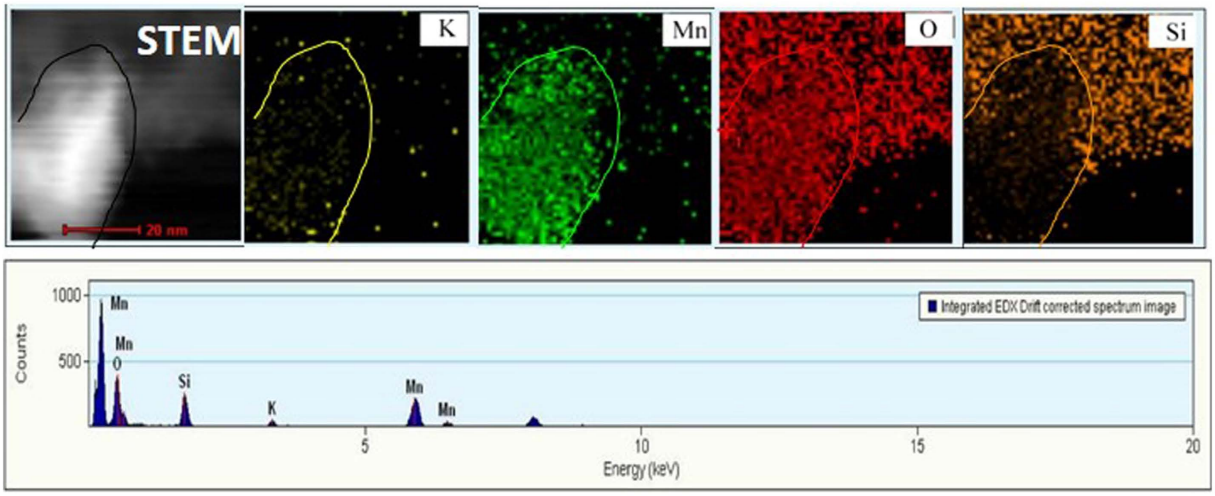

Figure 5. HAADF-STEM image and EDS elemental mapping of K-OMS-2/SiO_2-50.

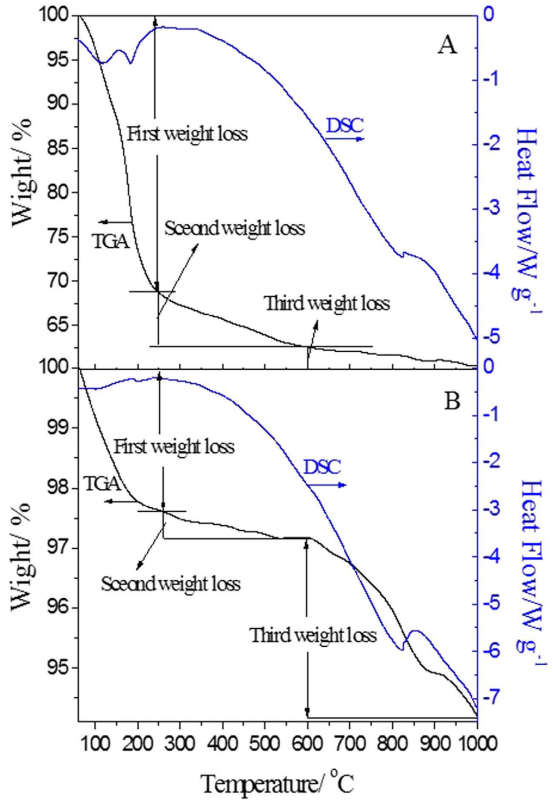

Figure 6. TG-DSC curves of K-OMS-2/SiO_2-50. (**A**) none calcined, (**B**) calcined.

of 600 °C. If the calcination temperature is over 600 °C, the crystal form of K-OMS-2 would be changed. The content of exchangeable active oxygen in the range of 250–600 °C may affect the physicochemical performances of as-prepared catalysts.

Raman spectra of As-prepared Catalysts. In an effort to investigate the influence of K doping on the microscopic structure and vibrational properties of MnO_x, Raman spectra of the K-OMS-2/SiO_2 with different K-OMS-2 loading amounts and 3DOM SiO_2 with different active components were measured, and the results are shown in Fig. 7. For the pure 3DOM SiO_2 (Fig. 7a), a weak Raman peak at about 492 cm^{-1} is observed, which is corresponding to the vibration of Si-O[33]. When the K-OMS-2 was loaded on the 3DOM SiO_2, five Raman peaks, including 637, 560, 482, 335 and 175 cm^{-1}, are observed in the Raman shift range of 150–1000 cm^{-1} [34]. The Raman peaks are maintained regular locations with increasing of K-OMS-2 loading. The peaks at 175 and 335 cm^{-1} can

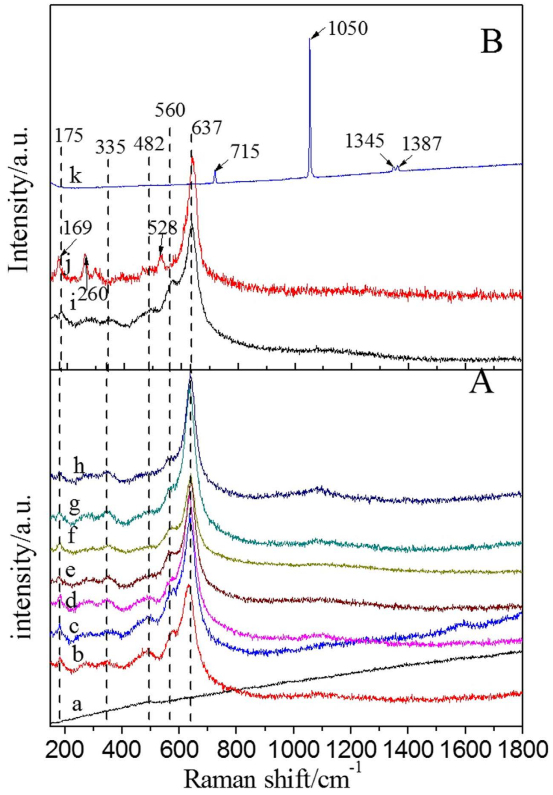

Figure 7. Raman spectra of as-prepared catalysts. (**A**) K-OMS-2/SiO_2 obtained at varied K-OMS-2 loadings: SiO_2 (a), K-OMS-2/SiO_2-10 (b), K-OMS-2/SiO_2-20 (**c**), K-OMS-2/SiO_2-30 (d), K-OMS-2/SiO_2-40 (e), K-OMS-2/SiO_2-50 (f), K-OMS-2/SiO_2-60 (g) and K-OMS-2/SiO_2-70 (h) (**B**) different support and active components on the 3DOMSiO_2: K-OMS-2/silica gel-50 (i), MnOx/SiO_2-50 (j) and KNO_3/SiO_2-50 (k).

be ascribed to the deformation modes of Mn-O-Mn, while the peaks at 637 and 560 cm^{-1} can be assigned to the Mn-O vibrations that are orthogonal and along the direction of the MnO_6 octahedral double chains[35,36]. The peak at 482 cm^{-1} (Raman shift of SiO_2) disappears when the mass ratio of KNO_3 and SiO_2 is exceeded 20%. This result indicates that the surface of SiO_2 is covered by K-OMS-2 nanoparticles, which agrees well with the results of SEM and TEM.

As shown in Fig. 7i, the Raman peaks of K-OMS-2/silica gel-50 are similar to that of K-OMS-2/SiO_2-50. Figure 7j shows Raman spectrum of MnO_x/SiO_2-50. Four bands can be observed at 639, 528, 260 and 169 cm^{-1} and they are assigned to Mn-O and Mn-O-Mn stretching mode of MnO_x, respectively. The MnO_2 and Mn_2O_3 components are contributed to the most intense Raman peak at 639 cm^{-1} [37]. Compared with the K-OMS-2/SiO_2, the Raman peak of Mn-O-Mn shifts to low wavenumber due to no influence of other ions. The Raman shifts of as-prepared catalysts in the Raman spectra demonstrate the doping of K in the OMS-2, this phenomenon also demonstrated by the XRD results (Fig. 1). The Raman peaks of KNO_3/SiO_2-50 are located at 715, 1050, 1345 and 1387 cm^{-1}. The 715 and 1050 cm^{-1} are belonged to the totally symmetric ν_1 and the doubly degenerate ν_4 modes of NO_3^-, respectively. The obvious difference in Raman peaks of KNO_3/SiO_2-50 and K-OMS-2/SiO_2-50 suggest that K ions have completely doped into the MnO_x and formed complex K-Mn oxides. The Raman spectra indicate that the weak Mn-O bands are obtained in the K-OMS-2 nanoparticles due to doping of K^+. Surface weak Mn-O bands are proposed to take part in activation of oxygen more easily. Therefore, the K-OMS-2/SiO_2 catalyst may show high catalytic activity than that of MnO_x/SiO_2.

H_2-TPR Results of As-prepared Catalysts. Catalytic combustion of soot is a complicated gas-solid (soot)-solid (catalyst) multi-phase reaction. The intrinsic redox properties of catalysts play a key role in the combustion of soot. Therefore, temperature-programmed reduction (TPR) by H_2 was used to measure these characteristics in the present work. As shown in Fig. 8, the peak position and types are similar for 3DOM K-OMS-2/SiO_2 with different K-OMS-2 loadings, while the intensity of H_2 consumption increases with the increasing of K-OMS-2 loading. For 3DOM SiO_2 (Fig. 8a), no reduction peak is observed. In the H_2-TPR profiles of 3DOM K-OMS-2/SiO_2 catalysts, there are three overlapping peaks (ranging from 250 to 700 °C), corresponding to a three-step reduction process. Reduction peaks are observed in three temperature ranges of 250–380 °C, 380–500 °C and 500–650 °C. Assuming that MnO is the final state in the reduction of OMS-2 Mn species[38]. The peak at 200–350 °C could be assigned to the reduction of MnO_2/Mn_2O_3 to Mn_3O_4, and the peak at 380–500 °C may be assigned to the reduction of Mn_3O_4 to MnO. The results indicate that substantial amount of Mn^{4+} and Mn^{3+} in K-OMS-2 can be reduced to Mn^{2+} below 500 °C, which is consistent with the previous reports[39]. The third reduction peak at 500–650 °C may be assigned to the reduction of K species. When the mass ratio of KNO_3 to SiO_2 is over

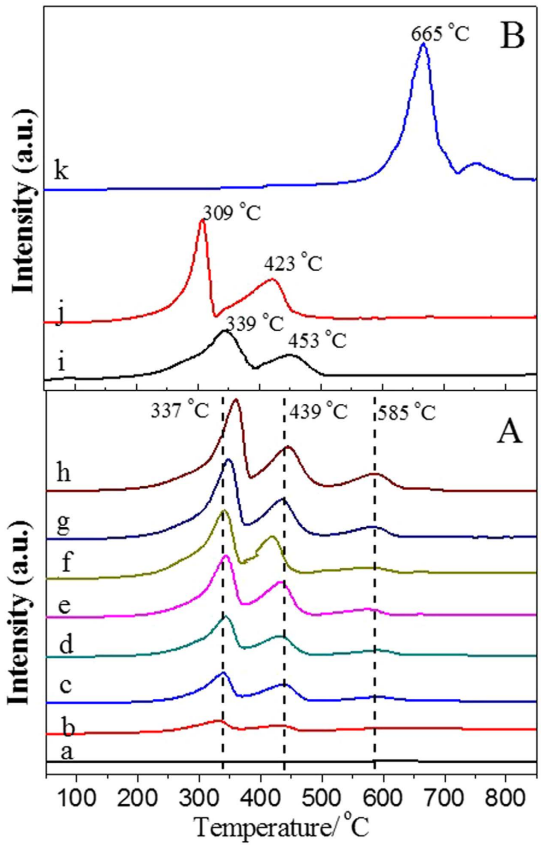

Figure 8. H_2-TPR curves of as-prepared catalysts. (**A**) K-OMS-2/SiO_2 obtained at varied K-OMS-2 loadings: SiO_2 (a), K-OMS-2/SiO_2-10 (b), K-OMS-2/SiO_2-20 (c), K-OMS-2/SiO_2-30 (d), K-OMS-2/SiO_2-40 (e), K-OMS-2/SiO_2-50 (f), K-OMS-2/SiO_2-60 (g) and K-OMS-2/SiO_2-70 (h); (**B**) different support and active components on the 3DOMSiO_2: K-OMS-2/silica gel-50 (i), MnO_x/SiO_2-50 (j) and KNO_3/SiO_2-50 (k).

25%, the intensity of K species reduction peak is obviously observed, and increases with increasing of K-OMS-2 loading amounts. The H_2-TPR profiles of K-OMS-2/silica gel, 3DOM MnO_x/SiO_2–50 and KNO_3/SiO_2 catalysts are presented in Fig. 8B. The peak position and types vary among the catalysts indicate different redox performance of as-prepared catalysts. Because of poor redox performance of SiO_2 supports and the same active components, the reduction peaks of K-OMS-2/silica gel-50 (Fig. 8i) are similar to that of 3DOM K-OMS-2/SiO_2-50. As for MnO_x/SiO_2-50, there are two main peaks at 309 °C and 423 °C, while no reduction peak is observed at relatively high temperature. It is apparent that the TPR peaks of 3DOM MnO_x/SiO_2-50 are present at lower temperature, indicating higher reducibility of manganese in MnO_x than the corresponding 3DOM K-OMS-2/SiO_2-50. The TPR profile of KNO_3/SiO_2-50 catalyst presents two important reduction signals at 530–720 °C and 720–830 °C assigned to the potassium nitrate reduction. The potassium nitrate can be reduced with H_2 to generate KNO_2, NO and NH_3. The presence of the H_2 consumption peak for KNO_3/SiO_2-50 indicates the presence of main KNO_3 species on the surface of 3DOM SiO_2 even after calcination at 550 °C. It is in good agreement with the XRD results of 3DOM KNO_3/SiO_2-50 (Fig. 1k).

XPS spectra of As-prepared Catalysts. XPS studies are conducted to gain insight into the oxidation state, surface composition, and atomic environment of K, Mn, O and Si species in the different samples, and the results are shown in Fig. 9 and Table 1. As shown in Fig. 9A, the K 2p spectrum consists of a spin-orbit split doublet composed of two peaks with an intensity ratio between K $2p_{3/2}$ and K $2p_{1/2}$ at about 2:1. The binding energies (BEs) of 292.4–292.8 eV and 295.2–295.6 eV are assigned to K $2p_{3/2}$ and K $2p_{1/2}$ (Table S2), respectively, which the separation of K $2p_{3/2}$ and K $2p_{1/2}$ peaks is about 2.6 eV[40]. The various binding energies of K indicates that environment of K is different in the as-prepared catalysts. Figure 9B displays the Mn 2p XPS of as-prepared catalysts. The Mn 2p spectra are significantly broadened and show some asymmetry towards both Mn $2p_{3/2}$ and Mn $2p_{1/2}$ peaks. Due to this feature, it is worth noting that the binding energies of components of as-prepared catalysts are in good agreement with the literature data reported for Mn^{3+} and Mn^{4+} [41]. As shown in Fig. 9B, the binding energies of the XPS Mn $2p_{3/2}$ peaks are found to be in the range 640.0–645.0 eV. Two kinds of Mn species including Mn^{3+} (ca. 641.5 eV), and Mn^{4+} (644.5 eV) are presented on the surface of as-prepared catalysts. Meanwhile, the Mn $2P_{1/2}$ peak also shows two kinds of Mn species in the BEs range of 650–655 eV (Table S2). The detailed peak fitting results of Mn 2p features for the two Mn ions are listed in Table 1. Apparently, the K-OMS-2 loadings have a slight impact on the surface Mn^{3+}/Mn^{4+} molar ratio. Table S2 indicates that the binding energies of Mn element decreased with increasing of K-OMS-2 loadings. The small change of BEs of Mn indicates the electronic densities

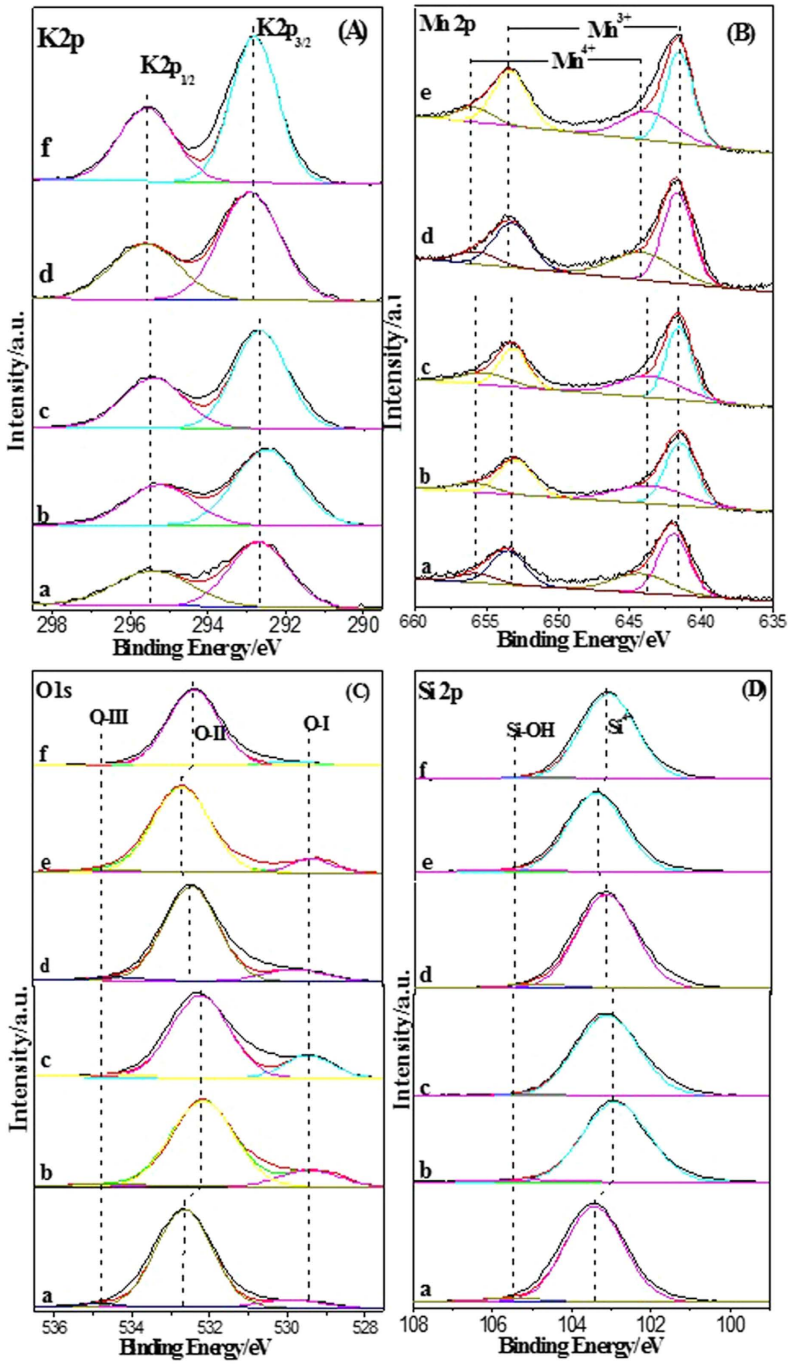

Figure 9. K 2p (**A**), Mn 2p (**B**), O1s (**C**) and Si 2p (**D**) XPS spectra of as-prepared catalysts (K-OMS-2/SiO_2-20 (a), K-OMS-2/SiO_2-50 (b), K-OMS-2/SiO_2-70 (c), K-OMS-2/silica gel-50 (d), MnOx/SiO_2-50 (e) and KNO_3/SiO_2-50 (f)).

of Mn atoms increase, suggesting that the low-valence Mn species increased[42]. Quantitative analysis of the surface components also proves that Mn species in the high loading of K-OMS-2 have lower average oxidation state than that of low loading catalyst[43]. Among those catalysts, because of the same K-OMS-2 loadings, the K-OMS-2/SiO_2-50 and K-OMS-2/silica gel-50 show similar surface Mn^{3+}/Mn^{4+} molar ratio (1.93 and 1.97, respectively), whereas MnO_x/SiO_2-50 is the lowest in terms of surface Mn^{3+}/Mn^{4+} molar ratio (1.65). More Mn^{3+} sites may be originated a weak Mn-O bond and formed more active oxygen species, which enhanced catalytic activity for redox reaction[42].

The corresponding spectra of oxygen species are presented in Fig. 9C. Three types of oxygen species, which are defined as O-I, O-II and O-III, can be observed from the XPS of O1s. The O-I component located at 529.5 eV are ascribed to lattice oxygen ions bonded to metal cations[44]. As shown in Fig. 9a–c, the type of O-I may be considered as mainly generated from Mn-O, K-O-Mn or some Si-O-Mn bonds in the K-OMS-2/SiO_2. The relative

Catalysts	Mn 2p R%		R%			R%	
	Mn^{3+}	Mn^{4+}	O-I	O-II	O-III	Si^{4+}	Si-OH
K-OMS-2/SiO_2-20	63.1	36.9	7.3	90.5	2.2	96.9	3.1
K-OMS-2/SiO_2-50	65.9	34.1	14.9	82.7	2.4	97.9	2.1
K-OMS-2/SiO_2-70	68.1	31.9	17.3	80.2	2.5	98.1	1.9
K-OMS-2/silica gel-50	66.3	33.7	11.5	85.8	2.7	95.7	4.3
MnOx/SiO_2-50	62.3	37.7	10.1	87.7	2.2	97.1	2.9
KNO_3/SiO_2-50	—	—	3.7	92.8	3.5	98.4	1.6

Table 1. Surface compositions and oxidation states of K, Mn, O and Si species calculated from XPS analyses. R%: the ratio of single component to total component.

Catalysts	T_{10}/°C	T_{50}/°C	T_{90}/°C	S_{CO2}^{m}/%	ΔT_{10}	ΔT_{50}	ΔT_{90}
pure soot	482	564	609	71.6	—	—	—
3DOM SiO_2	354	503	550	78.1	128	61	59
K-OMS-2/SiO_2-10	315	380	420	93.5	167	184	189
K-OMS-2/SiO_2-20	310	367	402	94.3	172	197	207
K-OMS-2/SiO_2-30	296	346	382	94.7	186	218	227
K-OMS-2/SiO_2-40	290	337	369	95.1	192	227	240
K-OMS-2/SiO_2-50	283	328	363	96.7	199	236	246
K-OMS-2/SiO_2-60	288	333	366	96.3	194	231	243
K-OMS-2/SiO_2-70	286	330	360	96.5	196	234	249
K-OMS-2/silica gel-50	336	381	423	96.1	146	183	186
MnO_x/SiO_2-50	301	359	397	96.9	181	205	212
KNO_3/SiO_2-50	312	365	389	92.5	170	199	220

Table 2. Catalytic performances of as-prepared catalysts for soot combustion. ΔT_{10}: The difference value of T_{10} between pure soot and catalysts, ΔT_{50}: The difference value of T_{50} between pure soot and catalysts, ΔT_{90}: The difference value of T_{50} between pure soot and catalysts.

intensity of O-I increases with the increasing of K-OMS-2 loading and the content of O-I increases from 0.073 to 0.173. The high content of O-I indicates that high loading of K-OMS-2 might produce more active oxygen species and show higher catalytic activity. Compared with the K-OMS-2/SiO_2-50, K-OMS-2/silica gel-50 shows somewhat lower content of O-I owing to parts of K-OMS-2 infiltrated into the inner of silica gel. Due to pure manganese oxide in the MnO_x/SiO_2-50, the BE of O-I has a small shift from 529.5 to 529.2 eV. The O-I content of MnO_x/SiO_2-50 is similar to that of K-OMS-2/silica gel-50. Because of no thermal decomposition of KNO_3, the KNO_3/SiO_2-50 shows lowest content of O-I and it occupies only 3.7%. The dominating O-II component at BE ~532.5 eV is obviously related to O^{2-} species in SiO_2 (Si-O-Si environments)[45]. The content of O-II decreases with increasing of K-OMS-2 loading due to more K-OMS-2 NPs on the surface of 3DOM SiO_2 at the high loading of K-OMS-2. Obviously, the O-II contents of as-prepared catalysts are related to the O-I, in other words, high O-I content is corresponding to low O-II. The minor O-III component located at ~534.6 eV may include contributions from Si-OH groups or adsorbed H_2O. In addition, in view of the catalyst composition, contribution of $-C=O$ groups (some adsorbent CO_2 is formed carbonate by K or Mn) is considered to be available. The KNO_3/SiO_2-50 shows the highest content of O-III, which is in good agreement with the results of Raman spectra. The Si 2p spectra of the catalysts (Fig. 9D) are dominated by a peak at BE~103.4 eV, characteristic of Si^{4+} in SiO_2; a smaller component at BE~105.5 eV indicates the presence of Si-OH species[46].

Catalytic Performances for Soot Combustion. The catalytic performances of 3DOM K-OMS-2/SiO_2 catalysts for soot oxidation were evaluated and the results are listed in Table 2. For comparison, the soot combustion reactions of without catalyst and over 3DOM SiO_2 were also estimated under the same reaction conditions. For the pure soot, the T_{10}, T_{50} and T_{90} are 482, 564 and 609 °C, respectively. 3DOM SiO_2 also shows somewhat catalytic activity for soot combustion, and the T_{10}, T_{50} and T_{90} are 354, 503 and 550 °C, respectively. This result indicates that the 3DOM structure of SiO_2 may enhance the contact area between soot and reaction gas. 3DOM K-OMS-2/SiO_2 catalysts show high catalytic activities for soot combustion. The catalytic activity enhanced with increasing of K-OMS-2 loading and reached maximum at a certain value (K-OMS-2/SiO_2-50). Further increasing the K-OMS-2 loadings, the catalytic activity almost keep constant. Compared the ΔT_{10}, ΔT_{50} and ΔT_{90} of K-OMS-2/SiO_2 catalysts in the Table 2, the ΔT_{10} of 3DOM K-OMS-2/SiO_2-50 catalyst is 199 °C, which is the highest among the 3DOM K-OMS-2/SiO_2 catalysts (i.e. the K-OMS-2/SiO_2-50 catalyst has the lowest initiation temperature). As shown in Table 2, the temperature of T_{90} decreases with increasing mass ratio of KNO_3 and SiO_2 and it is lower than 400 °C when the K loading is reached a certain value (K-OMS-2/SiO_2-30). Because of temperature range of 175–400 °C for diesel exhaust, soot particles over the K-OMS-2/SiO_2 catalysts can be completely burnt off when the diesel engines are normal running (i.e. the temperature of diesel exhaust is ca. 400 °C). In addition, the K-OMS-2/SiO_2 catalysts show higher CO_2 selectivity for soot combustion than that of

Catalysts	Reaction conditions		m_1/g[a]	m_2/g[b]	T_{10}/°C	T_{50}/°C	T_{90}/°C	S_{CO2}[m]/%	Refs
	NO/ ppm	O_2/%							
MnO_x	500	5	0.02	0.08	350	430	480	—	51
Ag/MnO_x	0	50	0.04	0.36	—	498	—	—	52
Ba/MnO_x-CeO_2	1000	10	0.01	0.1	362	393	—	99	53
$La_{1.6}Rb_{0.4}CuO_{4-\lambda}$	2000	5	0.01	0.1	429	505		96.3	54
KCu_2/Al_2O_3	600	5	0.125	0375	—	480	—	—	55
Pt/Al_2O_3	1000	10	0.01	0.1	—	464	—	>98	56
3DOM $LaCo_{0.5}Fe_{0.5}O_3$	2000	5	0.01	0.1	256	397	436	99.7	57
3DOM $Ce_{0.8}Zr_{0.2}O_2$	2000	5	0.01	0.1	348	396	424	—	58
3DOM $Au_{0.08}/LaFeO_3$	2000	5	0.01	0.1	229	359	—	99.7	14
3DOM $Au_{0.04}/Ce_{0.8}Zr_{0.2}O_2$	2000	5	0.01	0.1	218	356	404	99.7	59
3DOM $Pt_{0.08}/Ce_{0.8}Zr_{0.2}O_2$	2000	5	0.01	0.1	248	326	369	98.1	60
3DOM $Au_2@Pt_2/Ce_{0.8}Zr_{0.2}O_2$	2000	5	0.01	0.1	214	325	368	99.9	61
3DOM K-OMS-2/SiO_2-50	2000	10	0.01	0.1	283	328	363	96.7	This work

Table 3. Comparison between reported catalysts in referees and as-prepared catalyst for soot combustion under loose contact conditions. [a]mass of soot. [b]mass of catalyst.

pure soot combustion. All surpassed 90%. The selectivity to CO_2 increased with increasing of K-OMS-2 loading and the CO_2 selectivity value of K-OMS-2/SiO_2-50 catalyst is as high as 96.7%. In order to deeply investigate the interaction effect (K and Mn) and macropore effect for soot combustion, the catalytic activities of K-OMS-2/silica gel-50, 3DOM MnO_x/SiO_2-50 and 3DOM KNO_3/SiO_2-50 were tested and the results are shown in Table 2. Compared with 3DOM K-OMS-2/SiO_2-50, K-OMS-2/silica gel-50 shows much lower catalytic activity indicating that the 3DOM structure is favorable for soot combustion. It is attributed to that K-OMS-2 may be infiltrated into the inner of silica gel through accumulation porous (see the TEM image of Fig. S3), so that most of K-OMS-2 contact soot particle more difficultly than 3DOM K-OMS-2/SiO_2-50. 3DOM MnO_x/SiO_2-50 and KNO_3/SiO_2-50 show higher activity than K-OMS-2/silica gel-50 but lower than 3DOM K-OMS-2/SiO_2-50, indicating that the interaction effect between K and Mn has positive influence on soot combustion. In order to compare the catalytic performances of 3DOM as-prepared catalysts, the catalytic activities of previous other catalysts reported in literature are summarized in Table 3. When a comparison is made on catalysts for soot combustion, it must be noted that experimental conditions may be deviated from each other concerning reaction gas, catalyst dosage and measurement system. Thus, fine activity comparison of different catalysts is usually challenging. Nevertheless, a rough comparison, including the temperature for soot combustion, is still feasible. As shown in Table 3, the 3DOM K-OMS-2/SiO_2-50 catalyst showed lower temperature for T_{50} than the previous reported catalysts except the 3DOM $Pt_{0.08}/Ce_{0.8}Zr_{0.2}O_2$. From the Table 3, the K-OMS-2/SiO_2-50 gives the lowest T_{90}, i.e., the highest catalytic activity than other 3DOM metal oxides at high reaction temperature (i.e. comparison of T_{90}). In addition, the T_{90} of K-OMS-2/SiO_2-50 is much lower than 400 °C, indicating that the soot can be completely burnt off blew 400 °C. The temperature for complete catalytic combustion of soot is lower than the highest temperature of exhaust (175–400 °C), which is important for practical application. More importantly, the 3DOM K-OMS-2/SiO_2 catalysts were prepared by simple method and took very cheap KNO_3 and $Mn(NO_3)_2$ materials as active components. Obviously, non-noble metal catalysts show similar or even higher catalytic activities than noble metal catalysts in the medium and high temperature rage (see the Table 3). However, the as-prepared catalysts show lower catalytic activities than noble metal catalysts in the low temperature rage (temperature of T_{10}). The reason for this phenomenon is that the K-OMS-2 NPs have relatively lower redox property than noble metal catalysts for activation of oxygen species at low temperature (<300 °C). When the temperature is over 300 °C, a mass of oxygen can be activated and then the catalytic activities show great enhancement. This result is also well agreed with characterization of H_2-TPR (Fig. 8). Considering those factors, the catalytic activity of current 3DOM K-OMS-2/SiO_2 catalysts are significantly enhanced for soot combustion especially K-OMS-2/SiO_2-50 (T_{50} and T_{90} at ca. 328 °C and 363 °C). Therefore, 3DOM K-OMS-2/SiO_2 catalysts are promising for the practical application due to high catalytic activity and low cost.

Catalytic Performance of K-OMS-2/SiO_2-50 with Different Concentrations of NO in the Reactant Gases. In this work, in order to test and research the catalytic performance of as-prepared catalysts more deeply, the catalytic activities of K-OMS-2/SiO_2-50 with different concentrations of NO were also measured and the results are displayed in the Fig. 10. As shown in Fig. 10A, the profiles of CO_2 concentration over the K-OMS-2/SiO_2-50 show different tendencies under the condition of different concentration of NO. In the absence of catalyst, the temperature of highest CO_2 concentration is located at 580 °C. However, the temperature shifts to 450 °C when catalyst is presented. Moreover, the CO_2 profiles are higher and narrower than the case without NO. It suggested that the catalytic activities of K-OMS-2/SiO_2 are strongly affected by the NO gas. In order to more clearly describe the differences of catalytic activities under various concentrations of NO, the T_{10}, T_{50}, T_{90} and CO_2 selectivity are calculated and shown in Fig. 10B. The catalytic activity of 3DOM K-OMS-2/SiO_2-50 for soot combustion increases with increasing of concentration of NO when the NO is lower than 2000 ppm. However, the catalytic activity is almost kept constant when the NO is exceeded 2000 ppm. For comparison, the TPO

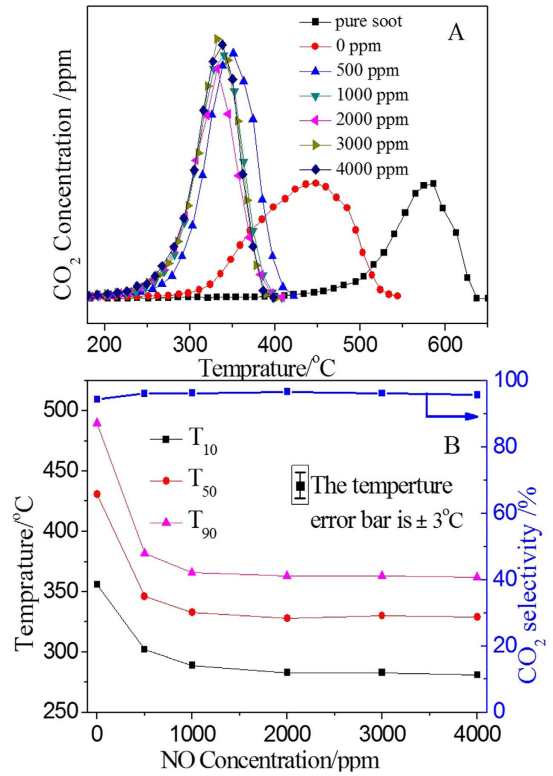

Figure 10. The CO_2 concentration profiles (**A**) and catalytic activities (**B**) of K-OMS-2/SiO_2-50 under different concentrations of NO (The temperature error bar is ±3 °C).

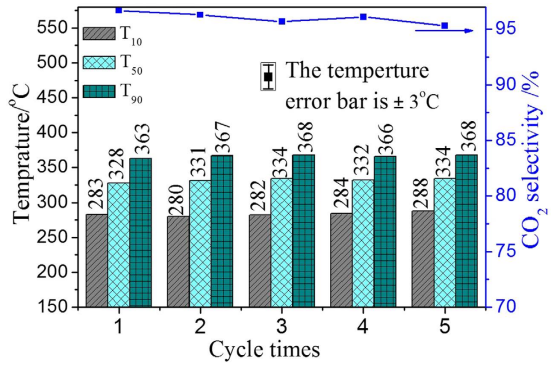

Figure 11. Tested stability results of 3DOM K-OMS-2/SiO_2-50 catalyst for soot combustion (The temperature error bar is ±3 °C).

result without NO is also included in Fig. 10B. Its T_{10}, T_{50} and T_{90} are 356, 431 and 490 °C, respectively. The result indicates that NO gas plays an important role in the soot combustion when its concentration is located at low value while high concentration has less assistance. As the same as reported in the previous literature[23], NO acts as an efficient mobile oxidizing agent, and the NO could be oxidized to NO_2 by oxygen during the reaction when catalysts are used. Since the oxidizing ability of NO_2 is stronger than that of O_2, the removal of soot particles by NO_2 is one of the main ways in soot combustion. Therefore, the soot combustion subtly changed solid (soot)-solid (catalyst) contact into solid (soot)-gas (NO_2)-solid (catalyst) contact. This altering reaction path greatly promotes soot combustion so that the catalysts show higher activities than that without NO[16]. More deeply explains will discuss in the following discussion.

Stability of 3DOM K-OMS-2/SiO_2-50 Catalyst. The stability of catalysts is one of the most important performances, especially in practical application. Therefore, the stability of 3DOM K-OMS-2/SiO_2-50 catalyst in five cycles running was examined and the results are shown in Fig. 11. 3DOM K-OMS-2/SiO_2-50 maintained high catalytic activity and CO_2 selectivity after five-cycle reaction under the condition of loose contact between catalysts and soot particles, the numerical values of T_{10}, T_{50} and T_{90} were 283 ± 5, 328 ± 6 and 363 ± 5 °C, respectively.

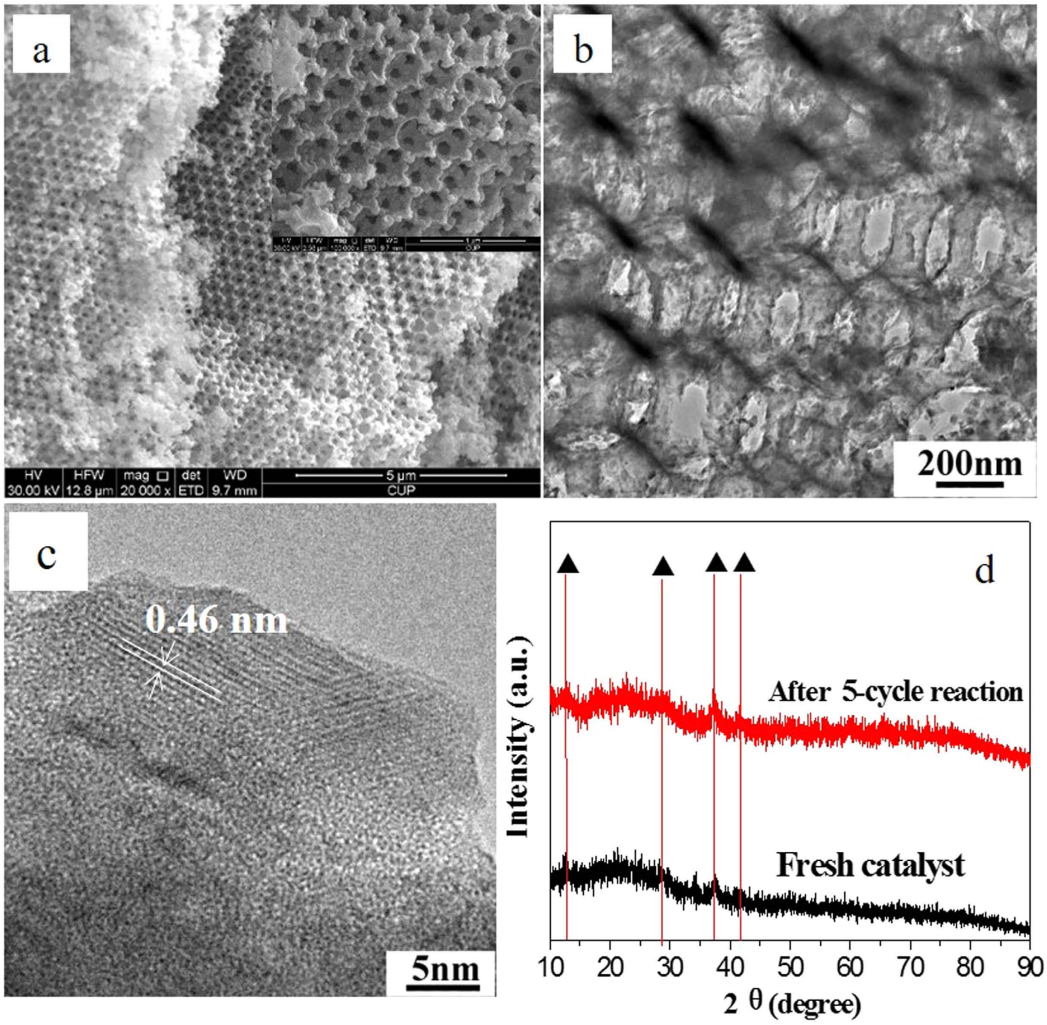

Figure 12. SEM (**a**), TEM images (**b,c**), and XRD (**d**), of 3DOM K-OMS-2/SiO_2-50 catalyst after 5-cycle reaction.

Meanwhile, the CO_2 selectivity value was more than 95% after reaction for five cycles. In this work, the 3DOM structure of SiO_2 support and K-OMS-2 nanoparticles play important roles in the catalytic combustion of soot. The used 3DOM K-OMS-2/SiO_2-50 catalyst was characterized by measurements of SEM, TEM and XRD and the results are listed in the Fig. 12. According to the SEM and TEM images of used 3DOM K-OMS-2/SiO_2-50 catalyst, 3DOM structure is not destroyed after five cycles reaction, and the mean size (23 ± 6 nm) of K-OMS-2 nanoparticles on the surface of 3DOM SiO_2 support is not remarkably changed in comparison with that of the fresh sample (24.25 ± 3.37 nm). The XRD similarity between used and fresh catalysts suggests that the crystal form and one-dimensional tunnel structure (0.46 nm) of K-OMS-2 are stable during the process of soot combustion. The characterization results of used catalyst indicate that 3DOM K-OMS-2/SiO_2 catalysts have good thermal stability and activity stability during soot combustion reaction.

Discussion

Macropores Effect of 3DOM SiO_2. It is well-known that the catalytic combustion of soot is a gas-solid-solid reaction, which the contact between soot and catalysts is one of the most important factors for improving the catalytic performance. In fact, many studies have demonstrated that the tight contact between soot and catalysts shows excellent catalytic performances for soot combustion[23]. However, loose contact between soot particles and catalysts is a typical way of contact in the process of after-treatment for diesel engine exhaust. Therefore, it is extremely important to study and design the active catalysts, which can improve the contact efficiency between the catalysts and soot particles under loose contact conditions. In order to enhance the contact efficiency, 3DOM materials with uniform pore size and periodic voids interconnected through open windows are designed and synthesized by colloidal crystal template method. As shown in Fig. S1a, the average diameter of ordered macroporous is about 310 nm and diameter of interconnected open windows is about 100 nm. Soot particles could easily across those pores and reach the active sites on the inner wall of 3DOM materials with the help of gas-flow Thus, 3DOM structures could enhance the contact between soot particles and catalysts.

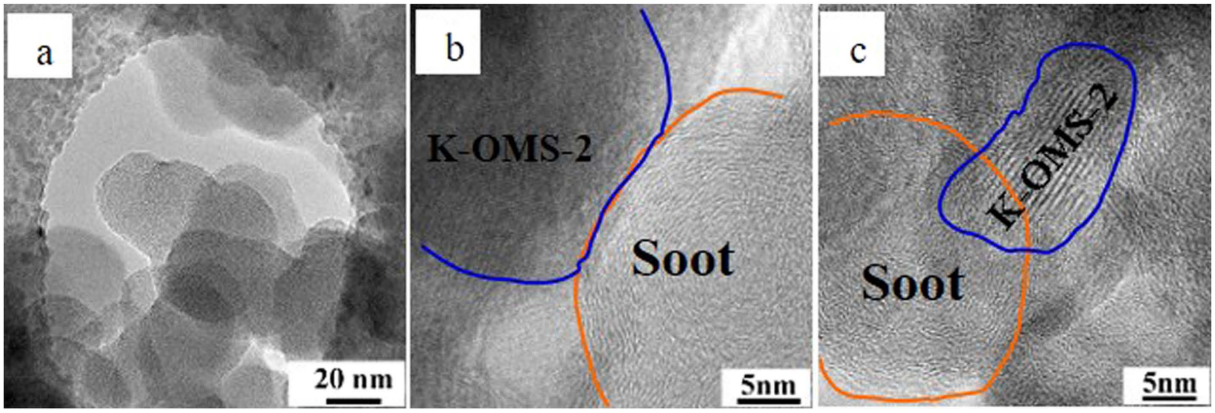

Figure 13. TEM (**a**), and HRTEM (**b,c**), images of 3DOM K-OMS-2/SiO_2-50 and soot complex. TEM image are obtained at the temperature 280 °C, reaction conditions: 10% O_2, 2000 ppm NO, Ar balance gas, total gas flow: 50 mL/min.

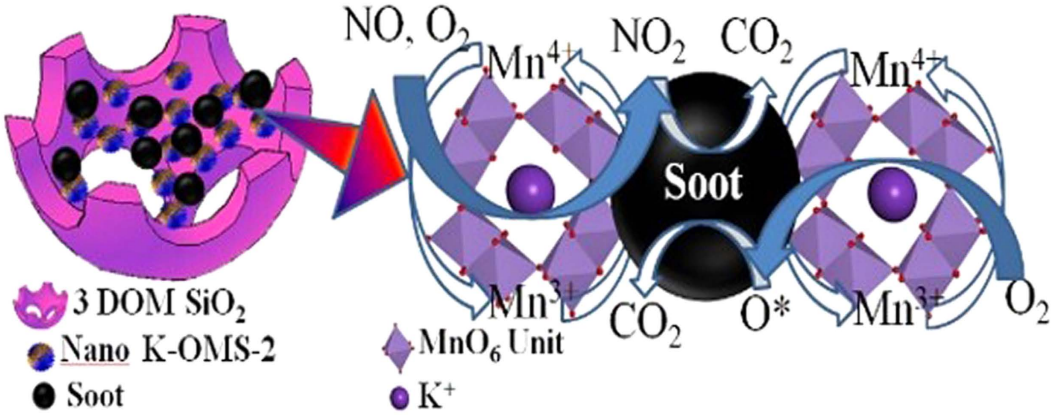

Figure 14. The reaction mechanisms of 3DOM K-OMS-2/SiO_2 catalyst for soot combustion.

In this work, in order to demonstrate the contact efficiency, the soot and 3DOM K-OMS-2/SiO_2-50 catalyst was studied under the same conditions for TPO reaction. In this confirmatory experiment, the reaction temperature of soot and 3DOM catalyst was programmed to 280 °C, which means the soot was not ignited. As we all know, the catalytic soot combustion is a gas-solid-solid reaction, which soot particles can enter the inner pores of 3DOM catalyst with the help of the reaction gas flow (O_2, NO and Ar) during the reaction process. More importantly, the rising reaction temperature may contribute to separating the agglomerate soot particles. Under the influence of gas flow and rising temperature, the soot particles can easily enter into the 3DOM structure and contact the inner active sites of 3DOM catalyst. As shown in Fig. 13a, the macropores of catalyst contacts with soot particles, indicating that 3DOM structure is a desirable feature for diesel soot combustion. This is the direct evidence that the perfect macroporous structure provides the ideal reaction place to solid reactants (diesel soot). As shown in HRTEM images (Fig. 13b and c), the soot and K-OMS-2 nanoparticles are well contact each other in the inner pores of 3DOM structure. Due to this contact efficiency, the number of available active sites of catalysts can be maximized for utilization, especially inner active sites of catalysts. More active sites would result in higher catalytic activity. The uniform macroporous network allows easy mass transfer and less diffusional resistance when the large size materials such as soot particles go through the catalyst structure. TEM results have intuitionally demonstrated that soot particles can easily enter the interior of 3DOM catalysts with the help of the airflow in the reaction process under the loose contact conditions, and have less resistance to go through the catalyst structure. In fact, our group has synthesized a series of 3DOM materials and they show higher catalytic activities than the corresponding particle materials[10,11,14]. Therefore, it is significantly important to study and design 3DOM structure for soot combustion.

Possible Reaction Mechanism for Soot Combustion on K-OMS-2/SiO_2 Catalyst. Based on all the results and analyses above, the potential mechanism schemes for soot combustion under presence/absence of NO are proposed and the possible mechanisms are shown in Fig. 14. When the NO is absent in the reaction system, soot oxidation occurred on the interface of K-OMS-2 nanoparticles and soot by the active oxygen species, which can be continuously supplemented by gaseous O_2 through the oxygen vacancies. Firstly, the gaseous O_2 is adsorbed on the active sites (i.e. oxygen vacancies on the surface of K-OMS-2), and then the adsorbed O_2 is

decomposed by redox reaction of Mn^{3+}/Mn^{4+} and formed active oxygen species(AOSs). Due to containing of K^+ in the tunnels of K-OMS-2, the electron clouds of K^+ may enhance the redox performance of Mn^{3+}/Mn^{4+} and lead to high production of AOSs. Thirdly, the AOSs are released from the surface of K-OMS-2 and migrated to the surface of soot. At last, the AOSs would be reacted with soot[47]. In this section, long distance between soot and K-OMS-2 would result in inactivation of AOSs. However, because of macropores effect of 3DOM structure, most of AOSs are fully exploited due to good contact between soot and K-OMS-2. As mentioned in the previous discussion, the reaction path of soot combustion has changed when NO is presented. The reaction mechanisms for the soot-NO-O_2 system can be proposed or summarized as follows. (1) The NO is oxidized to NO_2 by AOSs (released from the surface of K-OMS-2) in the gaseous atmosphere, and then strong oxidizing NO_2 migrated to the surface of soot and oxidized the soot. This way may be not played a major role in the system of soot-NO-O_2 due to inactivation of AOSs in the diffusion process; (2) Adsorption of gas phase O_2 and NO on the surface of catalysts. As revealed by XPS in the Fig. 9, due to changing valence state of Mn species (Mn^{3+}/Mn^{4+}) in the K-OMS-2, the oxygen vacancies are formed on the surface of catalysts, and then the active oxygen can be easily generated on the vacancies sites and formed chemisorbed oxygen[48]. Correspondingly, the NO was also interacted with surface active oxygen and formed bidentate/monodentate nitrates on the Mn^{n+} sites. Those bidentate/monodentate nitrates species were desorbed by formation of NO_2 from K-OMS-2, which acts as oxidant species for soot combustion via a spillover mechanism when temperature is increased. In this section, the doping of K^+ has significant influence on oxygen vacancies and NO adsorption. The intercalated K^+ leads to the mixed/averaged valence state of Mn^{4+} and Mn^{3+} are randomly distributed and easily transformed between Mn^{4+} and Mn^{3+}. The interaction between K^+ and Mn^{n+} contributes to forming AOSs and enhance catalytic activity[36]. (3) The special channel structure of K-OMS-2, which is larger than 0.46 nm, allows a lot of gas molecules to insert the channels. In this work, the dynamic diameters of NO and O_2 are 0.317 and 0.346 nm, respectively. Thus, the channel size of K-OMS-2 is suitable for adsorption of NO and O_2. In the channel of K-OMS-2, O_2 can be activated by the redox reaction of Mn^{3+}/Mn^{4+} and forms AOSs, and then the NO will be oxidized by AOSs to form NO_2. After that, the NO_2 is spread out from the tunnel structure and oxidizes the soot. In this section, a mass of gaseous NO molecules are spread into the tunnel structure owing to the adsorption of K^+. Therefore, a great number of gaseous NO molecules can be transformed into NO_2 to enhance the catalytic activity. More importantly, the K^+ ions are trapped in the 2×2 channels of K-OMS-2[49]. This structure guaranteed the stabilization of K^+ in the soot combustion. In the current work, as discussed above, the doping K^+ in the manganese oxides plays an essential role in the high catalytic activity for soot combustion.

Conclusions

A series of novel ordered micro/macro porous K-OMS-2/SiO_2 oxide catalysts, which contain 3DOM structure in the SiO_2 support and microporous structure in the nano-K-OMS-2, were firstly designed and successfully prepared by a very simple method. The average diameter of 3DOM SiO_2 is about 310 nm and microporous K-OMS-2 is about 0.46 nm. More interestingly, the microporous K-OMS-2 oxide nanoparticles with 20–25 nm are well dispersed and supported on the inner wall of the uniform macropores of SiO_2.

The as-prepared catalysts were firstly used in soot combustion reaction and they show high catalytic activities. Especially, the catalytic activities of as-prepared K-OMS-2/SiO_2 catalysts are similar to or even higher than those of the expensive noble metal catalysts in the medium and high temperature range. For example, the T_{50} of K-OMS-2/SiO_2-50, 328 °C, is much lower than those of Pt/Al_2O_3 and 3DOM Au/$LaFeO_3$, 464 and 356 °C, respectively. Moreover, the catalysts exhibited high catalytic stability for soot combustion. The macroporous effect of 3DOM structure is responsible for increasing the contact efficiency, the microporous effect of 2×2 tunnels of K-OMS-2 for adsorption of gas molecules and interaction of K and Mn for the activation of gas molecules, which are favorable for enhancing the catalytic activity for soot combustion. The K^+ ions are inevitably introduced into the microporous structure of OMS-2 and stabilized in the catalytic reaction. Meanwhile, the K^+ ions play an important role in templating and stabilizing the tunneled framework of OMS-2. The characterization results also prove that the catalytic activity of ordered hierarchical micro/macro porous K-OMS-2/SiO_2 catalyst is similar to that of fresh catalyst after five-cycle reaction.

Via the strategy of changing of K-OMS-2 loading and comparison of different active components, we successfully prepared a low cost, environmentally friendly, and highly active catalyst for soot combustion. The as-prepared catalysts are comparable to the expensive noble metal catalysts. This work should aid the rational design and facile preparation of highly efficient oxidation catalysts through the incorporation of other different cations into the tunnel of K-OMS-2. More importantly, the as-prepared micro/macro porous K-OMS-2/SiO_2 catalysts are promising for practical applications in the catalytic oxidation of diesel soot particles due to easy synthesis, low cost, high activity and stability.

Methods

Synthesis of Highly Well-defined PMMA Microspheres. The PMMA microspheres were synthesized by a modified emulsifier-free emulsion polymerization method[14]. The detailed synthesis steps are listed in the Supporting Information. (SEM images of PMMA microspheres and PMMA colloidal crystal templates are shown in Fig. S1).

Synthesis of 3DOM SiO_2. 3DOM SiO_2 was synthesized by colloidal crystal template (CCT) method with PMMA arrays as template and using tetraethyl orthosilicate (TEOS) as precursors[50]. In a typical procedure, 4.16 g TEOS was dissolved into the mixture of 2.5 mL water, 5 mL alcohol and 2.5 mL HCl aqueous solution (2 mol/L). After that, the hydrolyzation was proceeded in a water bath at 35 °C for 4 h. Then, 3 g PMMA arrays were impregnated into the above solution for 2 h. After complete impregnation, the PMMA arrays with the precursor solution were separated by vacuum filter and dried at 30 °C for 24 h. The dried samples were calcined to remove the CCT

in a tube furnace with an air flow (80 ml min^{-1}). The temperature-rising rate was 1 °C min^{-1} from room temperature to 600 °C, and the temperature of calcination at 600 °C was kept for 4 h, and then 3DOM SiO_2 supports were obtained.

Synthesis of 3DOM SiO_2-supported Microporous K-OMS-2 NPs. 3DOM K-OMS-2/SiO_2 catalysts were synthesized by incipient wetness impregnation method. In a typical procedure, a certain amount of KNO_3 and $Mn(NO_3)_2$ aqueous solution(50 wt%) were dissolved into deionized water, and then the above mixed aqueous solution was added into 3DOM SiO_2. In this step, the volume of KNO_3 and $Mn(NO_3)_2$ mixed aqueous solution should be equal to the pore volume of 3DOM SiO_2. After that, the impregnated sample was dealt with ultrasonic for 10 min and dried at 80 °C for 24 h. Then, the sample was calcined at 550 °C for 4 h in tube furnace and 3DOM K-OMS-2/SiO_2 catalysts were obtained. In order to obtain different K-OMS-2 loading amounts for K-OMS-2/SiO_2 catalysts, the weight ratio of K-OMS-2 to SiO_2 was changed. The as-prepared catalysts were defined as K-OMS-2/SiO_2-10, K-OMS-2/SiO_2-20 and K-OMS-2/SiO_2-30 for corresponding mass ratios of KNO_3 to SiO_2 were 5%, 10% and 15%, respectively. The dosages of raw materials are listed in the Table S1.

Synthesis of 3DOM MnO_x/SiO_2, KNO_3/SiO_2 and Powder K-OMS-2/silica gel. The detailed synthesis steps are described in the Supporting information.

Physical and Chemical Characterization. The characterization methods of X-ray diffraction (XRD), scanning electron microscopy (SEM), transmission electron microscopy (TEM), thermogravimetric analysis and differential scanning caborimetry (TG-DSC), Raman spectroscopy, H_2 temperature-programmed reduction (H_2-TPR) and X-ray photoelectron spectroscopy (XPS) are described in the Supporting information.

Activity Measurements. The catalytic performances of all the catalysts were evaluated with a temperature-programmed oxidation reaction (TPO) on a fixed-bed tubular quartz reactor ($\Phi = 8$ mm), and each TPO run from 150 to 650 °C at a 2 °C min^{-1} rate. The model soot was Printex-U particulates (diameter 25 nm, purchased from Degussa). Elemental analysis of Printex-U particulates showed its carbonaceous nature with 92.0% C, 0.7% H, 3.5% O, 0.1% N, 0.2% S and 3.5% others[14]. The catalyst (100 mg) and soot (10 mg) were mixed at a weight ratio of 10:1 with a spatula in order to reproduce the loose contact mode. Reactant gases (50 mL min^{-1}) contain 10% O_2 and 0.2% NO balanced with Ar. The outlet gas compositions were analyzed with an on-line gas chromatograph (GC, Sp-3420, Beijing) by using FID detectors. Before entering the FID detector, CO and CO_2 were fully converted to CH_4 by a convertor with Ni catalyst at 380 °C. The catalytic activity was evaluated by the values of T_{10}, T_{50} and T_{90}, which were defined as the temperatures at 10%, 50% and 90% of soot conversion, respectively. The selectivity to CO_2 formation (S_{CO2}) was defined as that the CO_2 outlet concentration (C_{CO2}) divided by the sum of the CO_2 and CO outlet concentration, i.e., $S_{CO2} = C_{CO2}/(C_{CO} + C_{CO2})$. S^m_{CO2} was denoted as S_{CO2} at the maximum temperature corresponding to the soot-burnt rate was the highest. In all TPO experiments, the reaction was not finished until the soot was completely burnt off.

References

1. Neeft, J. P. A., Makkee, M. & Moulijn, J. A. Diesel particulate emission control. *Fuel Process. Technol.* **47,** 1–69 (1996).
2. Twigg, M. V. Progress and future challenges in controlling automotive exhaust gas emissions. *Appl. Catal. B: Environ.* **70,** 2–15 (2007).
3. Heal, M. R., Kumar, P. & Harrison, R. M. Particles, air quality, policy and health. *Chem. Soc. Rev.* **41,** 6606–6630 (2012).
4. Liu, S. *et al.* Roles of acid Sites on Pt/H-ZSM5 catalyst in catalytic oxidation of diesel soot. *ACS Catal.* **5,** 909–919 (2015).
5. Xavier, L. P. S. *et al.* A. Simultaneous catalytic oxidation of carbon monoxide, hydrocarbons and soot with Ce-Zr-Nd mixed oxides in simulated diesel exhaust conditions. *Appl. Catal. B: Environ.* **162,** 412–419 (2015).
6. Yu, Y. F., Ren, J. L., Liu, D. S. & Meng, M. Domain-confined multiple collision enhanced catalytic soot combustion over a Fe_2O_3/TiO_2-nanotube array catalyst prepared by light-assisted cyclic magnetic adsorption. *ACS Catal.* **4,** 934–941 (2014).
7. Petkovich, N. D. & Stein, A. Controlling macro- and mesostructures with hierarchical porosity through combined hard and soft templating. *Chem. Soc. Rev.* **42,** 3721–3739 (2013).
8. Sadakane, M. *et al.* Facile preparation of three-dimensionally ordered macroporous alumina, iron oxide, chromium oxide, manganese oxide, and their mixed-metal oxides with high porosity. *Chem. Mater.* **19,** 5779–5785 (2007).
9. Liu, Y. X. *et al.* Au/3DOM $La_{0.6}Sr_{0.4}MnO_3$: Highly active nanocatalysts for the oxidation of carbon monoxide and toluene. *J. Catal.* **305,** 146–153 (2013).
10. Xu, J. F. *et al.* Easy synthesis of three-dimensionally ordered macroporous $La_{1-x}K_xCoO_3$ catalysts and their high activities for the catalytic combustion of soot. *J. Catal.* **282,** 1–12 (2011).
11. Zhang, G. Z. *et al.* Comparative study on the preparation, characterization and catalytic performances of 3DOM Ce-based materials for the combustion of diesel soot. *Appl. Catal. B: Environ.* **107,** 302–315 (2011).
12. Guillén-Hurtado, N., García-García, A. & Bueno-López, A. Active oxygen by Ce–Pr mixed oxide nanoparticles outperform diesel soot combustion Pt catalysts. *Appl. Catal. B: Environ.* **174–175,** 60–66 (2015).
13. Craenenbroeck, J. V. *et al.* Spectroscopic analysis of Au-V-based catalysts and their activity in the catalytic removal of diesel soot particulates. *J. Catal.* **209,** 515–527 (2002).
14. Wei, Y. C. *et al.* Highly active catalysts of gold nanoparticles supported on three-dimensionally ordered macroporous $LaFeO_3$ for soot oxidation. *Angew. Chem. Int. Ed.* **50,** 2326–2329 (2011).
15. Sun, Y. F. *et al.* The bifunctional catalyst of core-shell nanoparticles socketed on oxygen-deficient layered perovskite for soot combustion: *in-situ* observation of synergistic dual active sites. *ACS Catal.* **6,** 2710–2714 (2016).
16. Zou, G. C. *et al.* The synergistic effect in Co-Ce oxides for catalytic oxidation of diesel soot. *Catal. Sci. Technol.* **5,** 1084–1092 (2015).
17. Piumetti, M. *et al.* Contact dynamics for a solid-solid reaction mediated by gas-phase oxygen: Study on the soot oxidation over ceria-based catalysts. *Appl. Catal. B: Environ.* **199,** 96–107 (2016).
18. Piumetti, M., Bensaid, S., Russo, N. & Fino, D. Investigations into nanostructured ceria-zirconia catalysts for soot combustion. *Appl. Catal. B: Environ.* **180,** 271–282 (2016).
19. Huang, H. *et al.* Microwave-assisted hydrothermal synthesis of cryptomelane-type octahedral molecular sieves (OMS-2) and their catalytic studies. *Chem. Mater.* **22,** 3664–3669 (2010).
20. Luo, J., Zhang, Q. H., Garcia-Martinez, J. & Suib, S. L. Adsorptive and acidic properties, reversible lattice oxygen evolution, and catalytic mechanism of cryptomelane-type manganese oxides as oxidation catalysts. *J. Am. Chem. Soc.* **130,** 3198–3207 (2008).

21. Gálvez, M. E. *et al.* Influence of the surface potassium species in Fe-K/$A1_2O_3$ catalysts on the soot oxidation activity in the presence of NO_x. *Appl. Catal. B: Environ*. **152–153,** 88–98 (2014).
22. Ogura, M. *et al.* Carbonate-promoted catalytic activity of potassium cations for soot combustion by gaseous oxygen. *ChemCatChem* **6,** 479–484 (2014).
23. Kimura, R., Wakabayashi, J., Elangovan, S. P., Ogura, M. & Okubo, T. Nepheline from K_2CO_3/nanosized sodalite as a prospective candidate for diesel soot combustion. *J. Am. Chem. Soc.* **130,** 12844–12845 (2008).
24. Zhang, Z. L., Zhang, Y. X., Wang, Z. P. & Gao, X. Y. Catalytic performance and mechanism of potassium-supported Mg-Al hydrotalcite mixed oxides for soot combustion with O_2. *J. Catal.* **271,** 12–21 (2010).
25. Guo, X. *et al.* NO_x-assisted soot combustion over dually substituted perovskite catalysts $La_{1-x}K_xCo_{1-y}Pd_yO_{3-\delta}$. *Appl. Catal. B: Environ*. **142–143,** 278–289 (2013).
26. Gálvez, M. E., Ascaso, S., Moliner, R. & Lázaron, M. J. Me (Cu, Co, V)-K/Al_2O_3 supported catalysts for the simultaneous removal of soot and nitrogen oxides from diesel exhausts. *Chem. Eng. Sci.* **87,** 75–90 (2013).
27. Li, Q. *et al.* A unified intermediate and mechanism for soot combustion on potassium supported oxides. *Science report* **4,** 4725–4731 (2014).
28. Li, W. N. *et al.* Hydrothermal synthesis of structure- and shape-controlled manganese oxide octahedral molecular sieve nanomaterials. *Adv. Funct. Mater.* **16,** 1247–1253 (2006).
29. Sun, H., Chen, S., Wang, P. & Quan. X. Catalytic oxidation of toluene over manganese oxide octahedral molecular sieves (OMS-2) synthesized by different methods. *Chem. Eng. J.* **178,** 191–196 (2011).
30. Gandhe, A. R. *et al.* Manganese oxide OMS-2 as an effective catalyst for total oxidation of ethyl acetate. *Appl. Catal. B: Environ*. **72,** 129–135 (2007).
31. Deng, Y. Q., Zhang, T., Au, C. T. & Yin, S. F. Liquid-phase catalytic oxidation of p-chlorotoluene to p-chlorobenzaldehyde over manganese oxide octahedral molecular sieves. *Appl. Catal., A: Gen*. **467,** 117–123 (2013).
32. Li, Y. *et al.* Surface functionalization of SBA-15-ordered mesoporous silicas: Oxidation of benzene to phenol by nitrous oxide. *J. Catal.* **255,** 190–196 (2008).
33. Qiu, G. H. *et al.* Hydrothermal synthesis of manganese oxide nanomaterials and their catalytic and electrochemical properties. *Chem. Mater.* **23,** 3892–3901 (2011).
34. Polverejan, M., Villegas, J. C. & Suib, S. L. Higher valency ion substitution into the manganese oxide framework. *J. Am. Chem. Soc.* **126,** 7774–7775 (2006).
35. Wang, R. H. & Li, J. H. Effects of precursor and sulfation on OMS-2 catalyst for oxidation of ethanol and acetaldehyde at low temperatures. *Environ. Sci. Technol.* **44,** 4282–4287 (2010).
36. Kingondu, C. K. *et al.* Manganese oxide octahedral molecular sieves (OMS-2) multiple framework substitutions: A new route to OMS-2 particle size and morphology control. *Adv. Funct. Mater.* **21,** 312–323 (2011).
37. Kapteijn, F. *et al.* Alumina-supported manganese oxide catalysts: I. characterization: effect of precursor and loading. *J. Catal.* **150,** 94–104 (1994).
38. Sun, M. *et al.* Transition metal doped cryptomelane-type manganese oxide for low-temperature catalytic combustion of dimethyl ether. *Chem. Eng. J.* **220,** 320–327 (2013).
39. Yadav, G. D. & Mewada, R. K. Novelties of azobenzene synthesis via selective hydrogenation of nitrobenzene over nano-fibrous Ag-OMS-2 Mechanism and kinetics. *Chem. Eng. J.* **221,** 500–511 (2013).
40. Ousmane, M. *et al.* Highly selective direct amination of primary alcohols over a Pd/K-OMS-2 catalyst. *J. Catal.* **309,** 439–452 (2014).
41. Zhang, T. *et al.* Hierarchically multifunctional K-OMS-2/TiO_2/Fe_3O_4 heterojunctions for the photocatalytic oxidation of humic acid under solar light irradiation. *J. Hazard. Mater.* **243,** 302–310 (2012).
42. Liu, X. S. *et al.* Highly active CuO/OMS-2 catalysts for low-temperature CO oxidation. *Chem. Eng. J.* **162,** 151–157 (2010).
43. Hu, R. R. *et al.* Selective oxidation of CO in rich hydrogen stream over Ag/OMS-2 catalyst. *Int. J. Hydrogen Energy* **36,** 64–71 (2011).
44. Yu, X. H. *et al.* Facile controlled synthesis of Pt/MnO_2 nanostructured catalysts and their catalytic performance for oxidative decomposition of formaldehyde. *J. Phys. Chem. C* **116,** 851–860 (2012).
45. Castillo, R., Koch, B., Ruiz, P. & Delmon, B. Influence of the amount of titania on the texture and structure of titania supported on silica. *J. Catal.* **161,** 524–529 (1996).
46. Chenakin, S. P., Melaet, G., Szukiewicz, R. & Kruse, N. XPS study of the surface chemical state of a Pd/(SiO_2 + TiO_2) catalyst after methane oxidation and SO_2 treatment. *J. Catal.* **312,** 1–11 (2014).
47. Li, Z. Q. *et al.* Highly efficient multifunctional dually-substituted perovslcite catalysts $La_{1-x}K_xCo_{1-y}Cu_yO_3$ used for soot combustion, NO_x storage and simultaneous NO_x-soot removal. *Appl. Catal. B: Environ* **121–122,** 65–74 (2012).
48. Zhou, X. X. *et al.* Cu/Mn co-loaded hierarchically porous zeolite beta: a highly efficient synergetic catalyst for soot oxidation. *J. Mater. Chem. A* **3,** 9745 (2015).
49. Hou, J. T. *et al.* Tuning the K^+ concentration in the tunnel of OMS-2 nanorods leads to a significant enhancement of the catalytic activity for benzene oxidation. *Environ. Sci. Technol.* **47,** 13730–13736 (2013).
50. Yu, X. H. *et al.* Three-dimensionally ordered macroporous SiO_2 supported transition metal oxide catalysts: Facile synthesis and high catalytic activity for diesel soot combustion. *RSC Adv.* **5,** 49780–49790 (2015).
51. Becerra, M. E. *et al.* Soot combustion manganese catalysts prepared by thermal decomposition of $KMnO_4$. *Appl. Catal. B: Environ*. **102,** 260 (2011).
52. Guilhaume, N. *et al. In situ* investigation of diesel soot combustion over an $AgMnO_x$ catalyst. *Appl. Catal. B: Environ*. **119–120,** 287–296 (2012).
53. Wu, X. D., Liu, S., Lin, F. & Weng, D. Nitrate storage behavior of Ba/MnO_x-CeO_2 catalyst and its activity for soot oxidation with heat transfer limitations. *J. Hazard. Mater.* **181,** 722–728 (2010).
54. Liu, J. *et al.* The structures, adsorption characteristics of La-Rb-Cu-O perovskite-like complex oxides, and their catalytic performances for the simultaneous removal of nitrogen oxides and diesel soot. *J. Phys. Chem. C* **112,** 5930–5941 (2008).
55. Nejar, N., Makkee, M. & Gómez, I. M. J. Catalytic removal of NOx and soot from diesel exhaust: Oxidation behaviour of carbon materials used as model soot. *Appl. Catal. B: Environ*. **75,** 11–16 (2007).
56. Liu, S. *et al.* Sulfation of Pt/$A1_2O_3$ catalyst for soot oxidation: High utilization of NO_2 and oxidation of surface oxygenated complexes. *Appl. Catal. B: Environ*. **138–139,** 199–211 (2013).
57. Xu, J. F. *et al.* Three-dimensionally ordered macroporous $LaCo_xFe_{1-x}O_3$ perovskite-type complex oxide catalysts for diesel soot combustion. *Catal. Today* **153,** 136–142 (2010).
58. Zhang, G. Z. *et al.* Three dimensionally ordered macroporous $Ce_{1-x}Zr_xO_2$ solid solutions for diesel soot combustion. *Chem. Commun.* **46,** 457–459 (2010).
59. Wei, Y. C. *et al.* Three-dimensionally ordered macroporous $Ce_{0.8}Zr_{0.2}O_2$-supported gold nanoparticles: synthesis with controllable size and super-catalytic performance for soot oxidation. *Energy Envi*ron. *Sci.* **4,** 2959–2970 (2011).
60. Wei, Y. C. *et al.* Structural and synergistic effects of three-dimensionally ordered macroporous $Ce_{0.8}Zr_{0.2}O_2$-supported Pt nanoparticles on the catalytic performance for soot combustion. *Appl. Catal., A: Gen*. **453,** 250–261 (2013).
61. Wei, Y. C. *et al.* Multifunctional catalysts of three-dimensionally ordered macroporous oxide-supported Au@Pt core-shell nanoparticles with high catalytic activity and stability for soot oxidation. *J. Catal.* **317,** 62–74 (2014).

Acknowledgements

This work was financially supported by NSFC (21603149, 91545117, 21673142); 863 Program, (No. 2015AA034603); Liaoning Province Doctor Startup Fund, (201601150); Program of Excellent Talents in University, (51600208).

Author Contributions

Zhen Zhao proposed the idea and designed the research plan. Xuehua Yu carried out the experiments, collected the data and wrote the paper. Yuechang Wei and Jian Liu analyzed the experimental data and promoted the expression of English.

Additional Information

Supplementary information accompanies this paper at http://www.nature.com/srep

Competing Interests: The authors declare no competing financial interests.

How to cite this article: Yu, X. *et al.* Ordered micro/macro porous K-OMS-2/SiO_2 nanocatalysts: Facile synthesis, low cost and high catalytic activity for diesel soot combustion. *Sci. Rep.* **7**, 43894; doi: 10.1038/srep43894 (2017).

Publisher's note: Springer Nature remains neutral with regard to jurisdictional claims in published maps and institutional affiliations.